ACS APPLIED ENERGY MATERIALS

www.acsaem.org Article

Plasma-Assisted Mechanochemistry to Covalently Bond Ion-Conducting Polymers to Ni-Rich Cathode Materials for Improved Cyclic Stability and Rate Capability

Hyein Ko, Minsung Kim, Soo Yeong Hong, Jinhan Cho, Sang-Soo Lee, Jong Hyuk Park, and Jeong Gon Son*

Cite This: *ACS Appl. Energy Mater.* 2022, 5, 4808−4816 Read Online

ACCESS | Metrics & More | Article Recommendations | Supporting Information

ABSTRACT: Nickel-rich cathode materials in lithium-ion batteries are in the spotlight for high energy capacity, but they have the disadvantage of poor long-term stability due to interfacial phase changes and side reactions. We introduce a plasma-assisted mechanochemical composite process for covalently bonding polyvinylidene fluoride (PVDF) with high ionic conductivity to $LiNi_{0.8}Co_{0.1}Mn_{0.1}O_2$ (NCM811) particles in the dry-state electrode fabrication process. When plasma and mechanical friction are applied simultaneously, chemically inert PVDF is firmly and uniformly coated on NCM811 particles with a unique Ni−C covalent bond acting as an excellent cathode−electrolyte interface to inhibit transition metal dissolution and parasitic side reactions. In addition, PVDF has excellent ion conductivity and elasticity, so structural stability against the repetitive volume change can be achieved without interfering with lithium-ion transport. The PVDF-bonded Ni-rich cathode exhibits a high specific capacity of 215.2 mAh g^{-1} at 0.5 C, improved rate capability of 165.9 mAh g^{-1} at 5 C, and excellent cycle stability with a capacity retention of 83.6% after 300 cycles. This approach can maximize the electrochemical performance of conventional materials through one simple plasma-assisted composite process that controls the surface properties of cathode materials in the dry state.

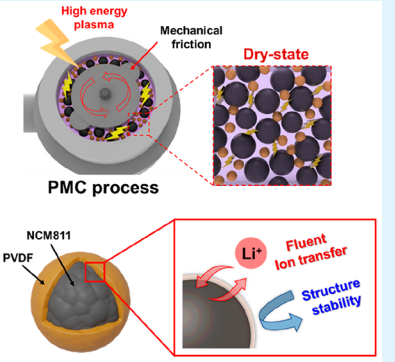

KEYWORDS: *plasma-assisted mechanochemistry, Ni-rich cathode, chemically bonded, lithium-ion battery, polyvinylidene fluoride, thin-film coating*

INTRODUCTION

Lithium-ion batteries (LIBs) are among the most widely used secondary battery systems due to their high energy density, cost-effectiveness, and environmental sustainability. The LIB is composed of an anode, cathode, electrolyte, and separator.[1,2] Among them, the energy density and stability of LIBs are greatly influenced by the cathode material, so many studies have been conducted to improve the electrochemical properties of the cathode material.[2] The layered lithium transition metal oxides ($LiTMO_2$ where TM is a transition metal, e.g., Ni, Co, Mn) are widely used as a representative material for cathode materials. Among them, high nickel $LiNi_{0.8}Co_{0.1}Mn_{0.1}O_2$ (NCM811) is considered as one of the most competitive products that can replace conventional LCO ($LiCoO_2$, ≈145 mAh g^{-1}) and LFP ($LiFePO_4$, ≈150 mAh·g^{-1}) due to its high practical capacity (>200 mAh g^{-1}) and low cost from the natural abundance of nickel.[3−5] Nevertheless, Ni-rich cathode materials like NCM811 have several challenges to overcome, including severe capacity degradation during long-term operation, poor rate capability, and thermal instability.[6] These problems are related to the high Ni content. Although an increase in the Ni content mainly improves the capacity, some disadvantages include cation mixing between Ni^{2+} and Li^+ ions resulting in Ni ion dissolutions, surface reconstruction, and residual lithium compounds.[7−9] These issues block the transport of Li^+ and electrons at the surface and impair the long-term cyclability due to side reactions with the electrolyte, which eventually lead to severe capacity fading during cycling and safety issues in batteries.[10,11]

In recent years, many attempts to overcome these significant limitations have been carried out on the cathode−electrolyte interfaces of Ni-rich cathode materials, including doping of bulk materials[12,13] and coating with various materials.[14−17] In particular, electrochemically inert inorganic materials such as Al_2O_3[18−20] or ZrO_2[21] or Li-ion conductive inorganic materials including $LiAlO_2$,[22] $LiAlF_4$,[23] Li_3PO_4,[24] and Li_2MnO_3[25] have been coated on the surface to suppress side reactions from the

Received: January 21, 2022
Accepted: March 16, 2022
Published: March 30, 2022

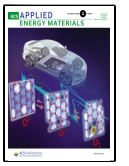

electrolyte and improve interfacial degradation. However, these hard coating materials are brittle with repetitive volume changes. Soft polymeric materials also can reduce irreversible phase transitions and improve cyclic stability by encapsulating Ni-rich anode materials, like rigid materials. In particular, conducting polymers such as PEDOT,[26] polypyrrole,[27,28] and polyaniline[29,30] for increasing electrical conductivity or elastic and adhesive Spandex[31] for structural stability against the volume changes have been coated. However, the coating materials should also consider the fluent ionic transport simultaneously, but it has hardly been considered; only coatings mixed with polyethylene glycol,[26,32] which have good ionic conductivity but form crystallites at lower than 55 °C, have been attempted. In addition, it is necessary to combine various methods to solve all these problems, and complicated processes with multiple steps inevitably take a long time, which is disadvantageous for mass production.

We focused on a mechanochemical technique that efficiently induces chemical reactions only at the surface for effective interfacial control between Ni-rich cathode materials and polymeric binders within a simple electrode fabrication process. The mechanochemistry process, which activates reactions using a mechanical force (strong shear, compressive, and friction forces), can enhance the affinity between different types of materials in a dry state;[33−35] thus, it has been applied to polymer nanocomposites, catalyst manufacturing,[36] and even dry electrode technology in battery fabrications.[34] In particular, the mechanochemistry process combined with plasma treatment, as known as the plasma-assisted mechanochemistry (PMC) process,[37−40] forms various functional groups on the surface of the materials by additionally introducing high-energy, plasma states of gas (O_2, N_2, Ar) in addition to mechanical frictions. This induces interfacial reactions and dramatically increases affinity between heterogeneous materials, such as covalent bonding. Several studies, including from our group,[37−40] have produced polymer nanocomposites,[41,42] electrocatalysts,[43] and graphene wrapped Fe_2O_3 for anodes[44] with enhanced interfacial affinity through the plasma-assisted composite process. However, the PMC process has rarely been applied to the fabrications of energy storage electrodes, especially cathode materials. We adopted a conventional polyvinylidene fluoride (PVDF) binder material as a composite material for the PMC process to maintain the battery manufacturing process without introducing new material. In addition, PVDF forms a stretchable and elastic gel with carbonate-based liquid electrolytes and has excellent ionic conductivity over 1×10^{-3} S cm^{-1} [45−47] so that the PVDF coating layer does not interfere and even can facilitate Li-ion transport on the surface of NCM811.

In this work, the PMC process was introduced as a single-step dry composite method of the conventional PVDF binder and the NCM811 microparticles to significantly improve the interfacial adhesions for structural stability of the Ni-rich cathode material without additional processes. In particular, in the PMC process, the surface of the chemically inert PVDF is functionalized through the plasma to form tight covalent bonds on the surface of the NCM811 particles, providing stable cathode−electrolyte interfaces and maintaining microstructures under repetitive volume changes over cycling. As a result, the PMC process overcomes the capacity limitations associated with parasitic side reactions with electrolytes, even in a wide range of polymer binder ratios from 3 to 20 wt %, and further improves specific capacity, rate performance, and cycle stability. Furthermore, this simple approach can easily enhance the electrochemical performances with only conventional materials through the plasma-assisted composite process that allows simple control of the surface properties of NCM811 in the dry state.

EXPERIMENTAL SECTION

Materials. All chemicals were directly used without additional purification. $Ni_{0.8}Mn_{0.1}Co_{0.1}O_2$ (NCM811; 8−10 μm) particles were purchased from MTI Corp. PVDF powder was acquired from Sigma-Aldrich, and its molecular weight and average diameter were 534 kg mol^{-1} and ∼270 nm. Single-walled carbon nanotubes (SWCNTs) from MEIJO eDIPS, EC grade of MEIJO Nanocarbon Co., Ltd., Nagoya, Japan, were used as a conductive additive for the fabrication of the electrode. *N*-Methyl-2-pyrrolidone (NMP; 99%, Sigma-Aldrich) was used as a dispersant of the composite materials.

Plasma-Assisted Mechanochemistry (PMC) Process. The PMC process was executed using a Nanocular system (Nanocular NC, HOSOKAWA Micron Ltd.) including a plasma processing device and a reaction chamber with a rotor to apply mechanical forces. First, the NCM811 and PVDF powders were placed between the chamber wall and the rotor. The weight ratio of NCM811 and PVDF was fixed at 8:2. While the chamber was evacuated, 20 sccm of O_2 gas was flowed to maintain a pressure of about 500 Pa. Then, a high voltage was generated at 1.5 kV with a plasma generator (HVT-100-20SS, Yamabishi Electric) during rotation for 1 h at 2300 rpm. During the process, the chamber was maintained in a cooled state by constantly circulating water.

Preparation of NCM811/PVDF Composites. After the PMC process, the dry mixtures were dispersed in NMP through mechanical stirring to obtain the PMC-processed composite paste and dispersion. To remove excess nonattached PVDF to NCM811, the above composite was vacuum filtered and washed with NMP several times to obtain the PMC-filtered composite. The filtered product was acquired in film and dried under a vacuum at 70 °C for 16 h. For the simply mixed samples, PVDF was mixed with pristine NCM particles using a Thinky mixer in a dry state at 20 and 3 wt %, respectively, and dispersed in NMP. To fabricate the electrodes, SWCNT, a conductive additive, was predispersed in NMP by tip sonication (90% amplitude, VCX-500, Youngjin Corp.) at a concentration of 4 wt % for 3 h. The PVDF/NCM composites dispersed in the NMP were mixed with the SWCNT dispersion in a solid content weight ratio of 95:5. The slurry was cast on an Al current collector (22 μm, MTI Corp.) using the doctor blade method and dried under vacuum at 70 °C for 16 h. The casted electrodes were cut to a size of 12 ⌀, and the mass loading of the active material was 4 mg cm^{-2} for both electrodes.

Material Characterization. Surface morphology and the status of the binder layer attached active material were measured by scanning electron microscopy (SEM) (Sigma 300, ZEISS). Before and after the charge−discharge cycle test, sampling to confirm the structural stability of the electrode was performed by an ion milling system (IMS) as a pretreatment device that mills a cross-section of the specimen using an argon ion with an acceleration voltage of 8 kV, and images were visualized by SEM. Element mapping was obtained using energy dispersive spectroscopy (EDS). The thickness of the binder layer attached active material was visualized with scanning transmission electron microscopy (STEM) (Talos F200X, Thermo Fisher Scientific) at an acceleration voltage of 200 kV. The element composition on the sample surface was characterized using X-ray photoelectron spectroscopy (XPS) (K-Alpha+, Thermo Fisher Scientific). The amounts of coated PVDF on NCM particles were quantitatively measured by thermogravimetric analysis (TGA; Q50, TA Instruments) from 30 to 700 °C at a heating rate of 10 °C min^{-1}.

Electrochemical Measurements. CR2032 coin-type cells (Wellcos Corp.) were assembled in an Ar-filled glovebox (KK-011AS, Korea Kiyon). Lithium metal foil (0.6 mm × 39 mm, Wellcos Corp.) was used as an anode for assembled half cells. Polyethylene (Celgard 3501, 66 mm) and 1 M $LiPF_6$ in EC (ethylene carbonate)/DMC (dimethyl carbonate) (1/1 = v/v) with 7.5 wt % FEC (fluoroethylene

https://doi.org/10.1021/acsaem.2c00244
ACS Appl. Energy Mater. 2022, 5, 4808−4816

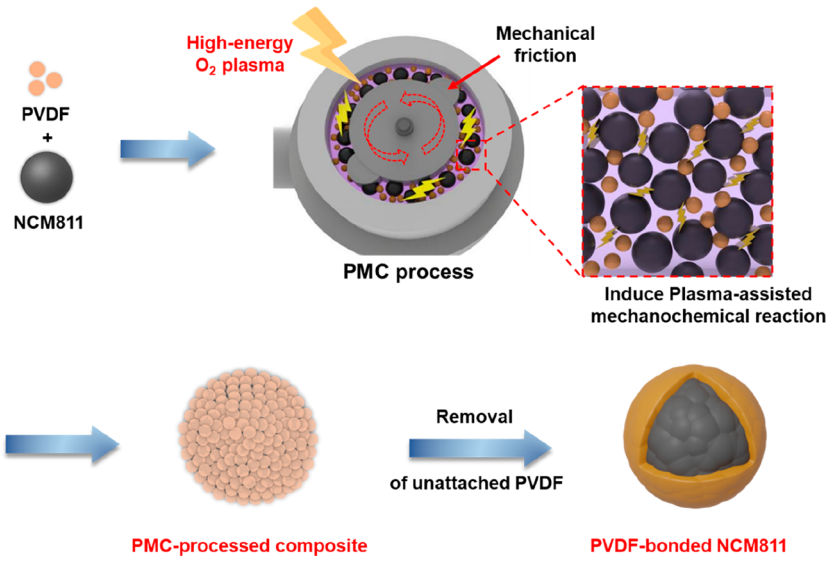

Figure 1. Schematic illustration of the plasma-assisted mechanochemistry (PMC)-based NCM811/PVDF composite fabrication process. During the process, a powerful mechanical force was applied by the rotor rotating in the chamber, and high-energy plasma states of O_2 gas were simultaneously applied to the mixture.

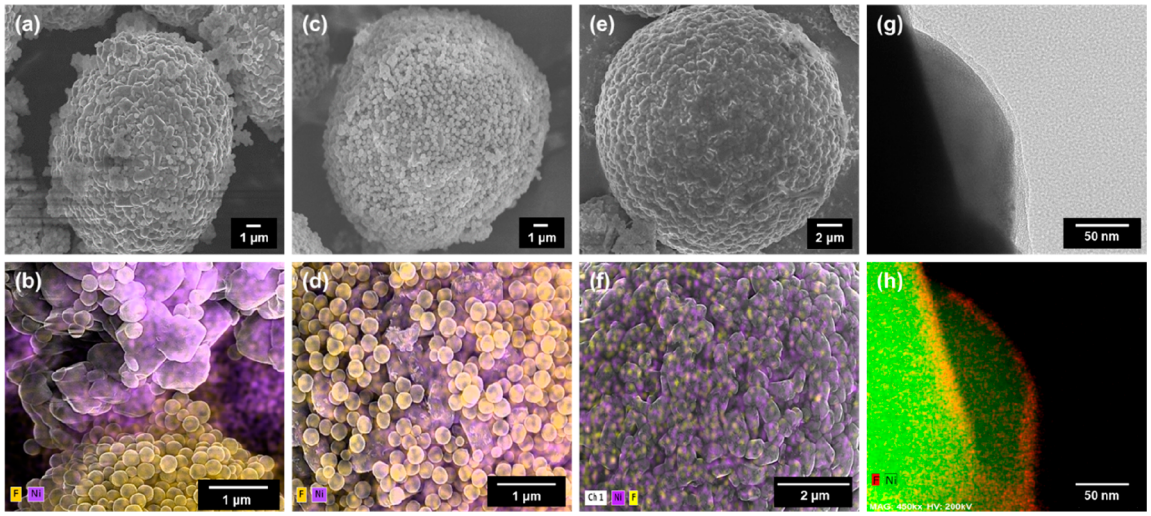

Figure 2. (a–f) SEM images and their EDS mapping images showing the distribution of chemical elements (Ni, F) of (a and b) simply mixed NCM811 and PVDF powders, (c and d) the PMC-processed NCM811/PVDF composite, and (e and f) PMC-filter processed PVDF-coated NCM811 particles. (g and h) TEM image and its EDS image of the PMC-filter processed PVDF-coated NCM811 particle.

carbonate; an additive to prevent lithium dendrite formation in the lithium metal anodes) from Wellcos Corporation were used as a separator and an electrolyte, respectively. Cell tests were performed for each cycle in the potential range over 3.0–4.3 V (vs Li/Li^+) by applying the galvanostatic charge–discharge mode of a battery cycler (WBCS 3000, WonAtech) at 25 °C and 40% humidity in a constant temperature and humidity device. Before the electrochemical properties were tested, the first cycle of all cells was conducted at a scan rate of 0.1 C (1 C = 185 mA g^{-1}) to form a stable SEI layer. Then, cyclability tests were carried out at 0.5 C, and rate capability was tested for various C-rates from 0.1 to 5 C. EIS analysis was performed at an amplitude of 10 mV on a galvanostat (Autolab PGSTAT101, Metrohm AG) with NOVA software over the frequency range of 0.01 Hz to 10 MHz.

■ RESULTS AND DISCUSSION

Figure 1 illustrates a schematic diagram of the NCM811/PVDF composite fabrication via the PMC process. The PMC process simultaneously applies mechanical friction of rotating blades and high-energy oxygen plasma to introduce various functional groups to the surface of the materials and further induce reactions at the interface between the electrode materials to form covalent bonds. The NCM811 and PVDF powders are placed in a chamber with two blunt blades and rotated to apply mechanical friction. Since the interface between two different materials is mechanically rubbed, the ratio should be at least a certain amount to be effective, so the mass ratio was fixed at 8:2. While the blade rotated at 2300 rpm for 60 min, which is gentle enough to prevent NCM particles from breaking, the chamber's pressure was maintained at 10^2–10^3 Pa with oxygen gas, and a high voltage of 1.0–1.5 kV was applied to generate a high-energy plasma in the chamber. After the PMC process, the surface of the NCM particles was densely covered with PVDF particles. To remove excess PVDF chains not attached to the NCM particles, a filtration process was performed with NMP, which is a good

https://doi.org/10.1021/acsaem.2c00244
ACS Appl. Energy Mater. 2022, 5, 4808–4816

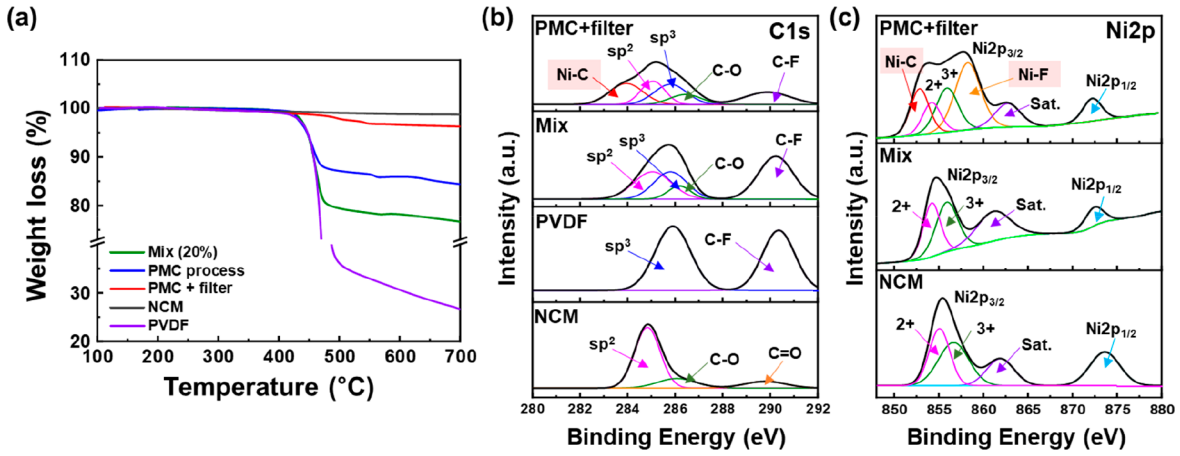

Figure 3. (a) TGA curve and XPS spectra for (b) C 1s and (c) Ni 2p of mixed composites, PMC-filtered composites, and pristine NCM811 and PVDF particles.

solvent for PVDF. After the filtration process, PVDF-coated NCM811 particles in which PVDF was chemically bonded to the surface of the NCM811 particles could be obtained.

The morphologies of the NCM811/PVDF composites by simple dry mixing, the PMC process, and filtration after the PMC process were observed by scanning electron microscopy (SEM) and energy-dispersive X-ray spectroscopy (EDS) analysis in Figure 2. The pristine PVDF and NMC811 particles are shown in Figure S1, and their diameters are 272 ± 2 nm and ∼10 μm, respectively. Figure 2a shows a SEM image of simply mixed NCM811 and PVDF composites at a ratio of 8:2 using a Thinky mixer in the dry state for 5 min. The PVDF particles were mainly located between the NCM811 particles and acted as binders. However, as shown in the EDS mapping image in Figure 2b, nickel domains from NCM and fluorine domains from PVDF exist separately, showing irrelatively agglomerated and uneven distribution. On the other hand, as shown in Figure 2c, the PMC-treated NCM811/PVDF composite was densely and uniformly covered with spherical PVDF particles on the round surface of the NCM811 particles. While the size of pristine PVDF particles is 272 ± 2 nm, after the PMC process, there is a size reduction of about 3% to the level of 265 ± 2 nm, so the degradation ratio is negligible. The EDS mapping image (Figure 2d) also showed that Ni and F elements were well distributed, demonstrating that the PVDF particles uniformly adhered to the NCM811 particle surface. Figure S2 also shows that the PVDF particles are evenly distributed on the NCM811 particles after performing the plasma-free mechanical friction process for the same amount of time. After the filtration process to remove excess PVDF not attached to NCM, a thin polymer layer was observed on the surface of the NCM811 particles, as shown in Figure 2e. In addition, in the EDS mapping image of Figure 2f, the F element of PVDF appeared on the entire surface of the NCM811 particles, and in the TEM images of Figures 2g,h and S3, the NCM811 particles were covered with an ∼15 nm thick layer of PVDF. Therefore, it is confirmed that PVDF formed a thin and tightly attached coating layer on NCM811. However, after the plasma-free mechanochemical process, it was confirmed from the SEM and EDS map images in Figure S4 that almost no PVDF remained on the surface of the NCM particles after the filtration process.

To investigate the amount of PVDF in the NCM811/PVDF composites, a thermogravimetric analysis (TGA) analysis was carried out at a heating rate of 5 °C min^{-1}. TGA curves of the pristine NCM811 and PVDF, simply mixed composites, PMC-processed composites, and PMC-filter processed composites are displayed in Figure 3a. The weight losses of pristine NCM811 and pristine PVDF up to 700 °C were 1.0% and 73.3%, respectively. The weight loss from 400 to 700 °C from PVDF of the PMC-processed sample (15.7%) was slightly lower compared to that of the untreated mixed sample (21.3%); it is presumed to be due to the loss after use from the mechanical friction equipment and the partial degradation or cross-linking (forming ash) of the polymers by the plasma. The PMC-filtered composite exhibited a meaningfully reduced weight loss (∼2.3 wt %) due to the large amount of excess PVDF chains not being attached to the NCM particles removed by filtration but still having a small amount of PVDF attached to NCM. A certain amount of PVDF remained even after filtration with NMP, a very good solvent for PVDF, which means that the remaining PVDF chains are strongly attached to the NCM particles. The actual PVDF content of the filtered sample was calculated to be 3% by weight compared to the weight loss of pristine NCM. However, when the plasma-free mechanochemical process was performed, the weight loss was almost the same as that of pristine NCM, indicating that PVDF was hardly attached after the filtration process (Figure S5).

To investigate the effect of plasma on the chemical structure of the composites in the PMC process, X-ray photoelectron spectroscopy (XPS) spectra of the NCM811/PVDF composites prepared by various methods were analyzed in Figure 3b,c. In the full scan of the XPS spectra, the oxygen fraction significantly increases from 5% in mixing to 9.3% after the PMC process to 25.9% after filtration due to oxygen plasma treatment, while the fraction of the F element in XPS of the simply mixed electrode was 46% and gradually decreased to 33.7% after the PMC process and 27.7% after filtration. In the spectrum of C 1s in Figure 3b, pristine PVDF showed a CH_2 peak at 285.5 eV and a CF_2 peak at 290.0 eV with the same intensity, and pristine NCM exhibited the graphitic sp^2 carbon peak at 284.8 eV produced during high-temperature synthesis. While the 3 wt % mixed composite showed a spectrum in which the above three peaks overlapped, the PMC-filtered sample exhibited a new peak at 283.7 eV due to Ni−C bonding[48,49] caused by mechanical friction and the plasma effect at the interface. It is known that direct carbon−nickel bonding at the polymer−metal interfaces can only occur via

https://doi.org/10.1021/acsaem.2c00244
ACS Appl. Energy Mater. 2022, 5, 4808−4816

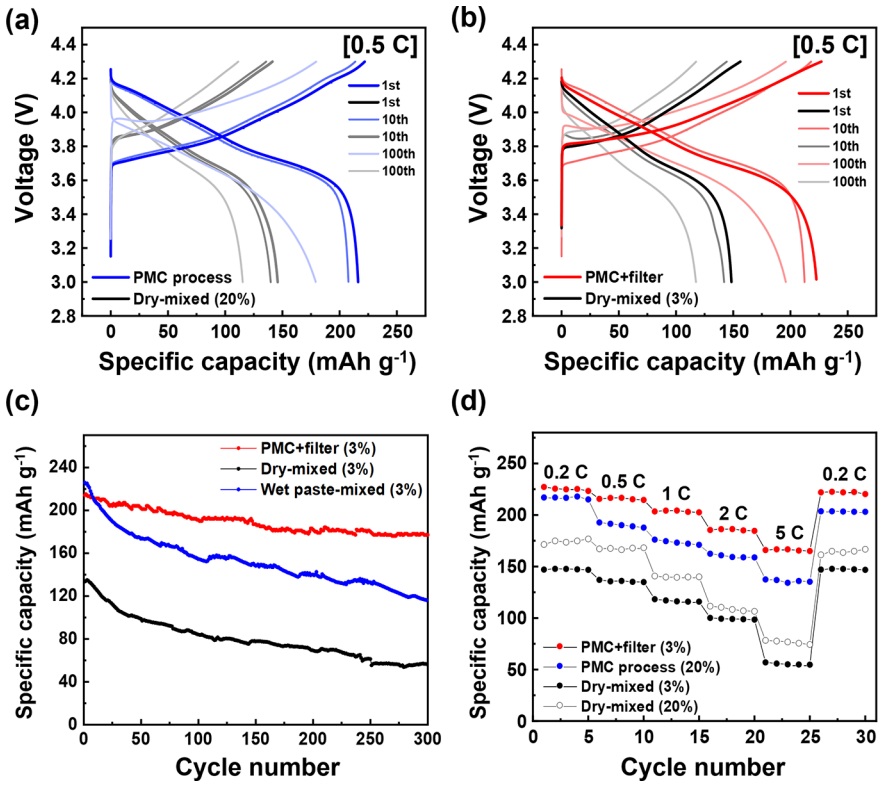

Figure 4. (a, b) Initial charge−discharge curves and charge−discharge curves at the 10th and 100th cycles of simply mixed (3 and 20 wt % of PVDF contents), PMC-processed, and PMC-filtered NCM/PVDF electrodes at 0.5 C. (c) Cycling performances at 0.5 C up to 300th cycles of conventionally prepared wet paste-mixed, dry-mixed (3 wt %), and PMC-filtered NCM/PVDF electrodes. (d) Rate capabilities at different current rates of mixed (3 and 20 wt %), PMC-processed, and PMC-filtered NCM/PVDF electrodes. All measurements are conducted in the voltage range of 3.0−4.3 V vs Li/Li^+.

plasma-included processes[48,49] and be used for strong adhesion of polymer−metal interfaces. There is a report of increasing the high adhesion between metal and fluoride polymer by depositing PTFE on nickel through plasma sputtering, and the Ni−C bond was confirmed by XPS.[48] A plasma technique for greatly increasing the low adhesion between metals and fluorine polymers is widely used in the industry. On the basis of these results, it was found that high energy on the PVDF surface in the plasma-composite process (plasma-assisted mechanochemistry, PMC) breaks the bond between C−H and C−F to form carbon radicals, and these radicals covalently bond with the oxygen or metal surface of the NCM particles to form strong adhesion.[50] Furthermore, the C−O peak at 285.8 eV was also observed due to the polymer oxidation from O_2 plasma. In the spectrum of Ni 2p in Figure 3c, pristine NCM811 and mixed composites identically showed Ni $2p_{3/2}$ peaks of Ni^{2+}/Ni^{3+} at 856.0 and 874.2 eV, Ni $2p_{1/2}$ peaks, and their satellite peaks. However, the PMC-filtered composite additionally showed a clear Ni−C peak at 853.0 eV as evidence of chemical bonding and a stronger and broader Ni−F peak at 862.5 eV compared to the the previous $2p_{3/2}$ peak. The F 1s and O 1s spectra in Figure S6 also showed that the PMC-filtered composite exhibited a new metal−F peak at 684.9 eV, C−F peak of PVDF at 688.5 eV, and an enhanced C−O peak at 531.1 eV by O_2 plasma. These changes in chemical bonds indicate that the PMC process directly forms strong covalent bonds at the interface between the polymer and NCM particles through the intimate interactions of plasma and strong frictional forces.

To measure electrochemical performance, simply mixed (PVDF fraction of 20 and 3 wt %), PMC-only, and PMC-filtered NCM/PVDF composite cathodes were fabricated by adding single-walled carbon nanotubes with a 95:5 ratio as a conductive additive and coating the pastes dispersed in NMP on Al foils. Then, the electrochemical performance was evaluated by assembling the NCM/PVDF composite cathodes into coin cells with lithium foil as the counter electrode and 1 M $LiPF_6$ in EC (ethylene carbonate)/DMC (dimethyl carbonate) (1/1 = v/v) with 7.5 wt % FEC (fluoroethylene carbonate) as the liquid electrolyte. Figure 4a,b shows the initial, 10th, and 100th cycles of charge−discharge curves of the samples at 0.5 C (1 C = 185 mAh g^{-1}) between 3.0 and 4.3 V. The 20 and 3 wt % simply mixed NCM/PVDF samples exhibit relatively lower initial discharge capacities than the theoretical capacities of 149.8 and 148.3 mAh g^{-1}, respectively, due to the less optimized electrode structures. However, the initial discharge capacities of PMC-processed and PMC-filtered electrodes showed considerably high values of 205.8 and 215.2 mAh g^{-1}. In addition, the charge−discharge capacities in the 100th cycles of the simply mixed samples showed relatively low capacity retentions of 81.3% (20 wt %) and 66.8% (3 wt %), while the PMC-processed and the PMC-filtered samples showed high-capacity retentions of 89.3% (184.7 mAh g^{-1}) for PMC and 90.3% (188.9 mAh g^{-1}) for PMC-filtered samples without significant changes of the curves at 10th and 100th cycles, respectively.

Figure 4c shows the cycling performance of 3 wt % simple mixing and PMC-filtered NCM/PVDF electrodes at 0.5 C. The 3 wt % simple mixing electrode decreased capacity at a

https://doi.org/10.1021/acsaem.2c00244
ACS Appl. Energy Mater. 2022, 5, 4808−4816

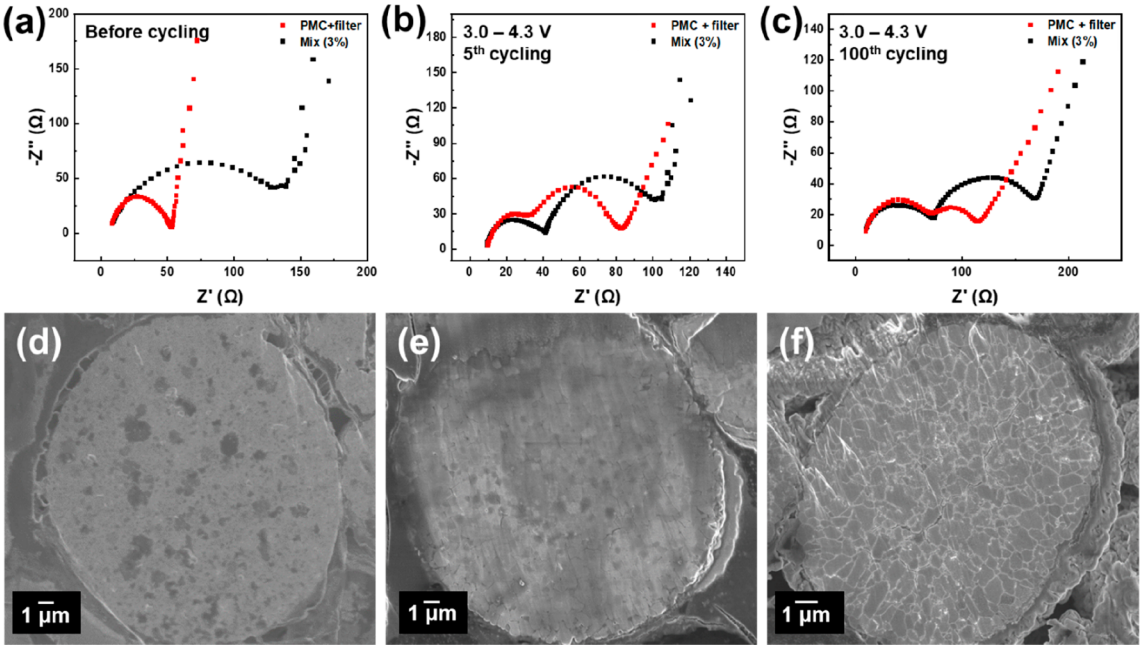

Figure 5. (a–c) EIS spectra of simply mixed (3 wt %) and PMC-filtered electrodes measured at 25 °C (a) before and (b) after 5 cycles and (c) 100 cycles of charging–discharging. (d, e) SEM images of the PMC-filtered electrodes (d) at the pristine state and (e) after 100 cycles. (f) SEM images after 100 cycles of the no PMC, simply mixed (3 wt %) NCM/PVDF electrodes.

relatively rapid rate, showing capacity retention of 42.3% after 300 cycles. The conventionally prepared NCM/PVDF electrode from wet paste mixing with NMP showed a capacity of 221.3 mAh g^{-1} in the initial charge–discharge but a relatively rapid capacity decrease, exhibiting 161.2 mAh g^{-1} (capacity retentions of 72.8%) at 100th cycles. In contrast, the PMC-filtered sample exhibited a superior discharge capacity of 180.1 mAh g^{-1} and an extremely high capacity retention of 83.6% after 300 cycles compared to other high-Ni cathodes. The 20 wt % simple mixing and PMC-processed electrodes also showed similar results (Figure S7). The cells were evaluated to investigate the rate capabilities by operating 5 cycles at each rate with gradually increasing the rate from 0.2 to 5 C and back to 0.2 C, as shown in Figure 4d. Compared to the simply mixed electrodes, whose performance decreased significantly with an increase in rate, the capacity of the PMC-filtered electrode was outstandingly maintained at 225.7, 215.5, 203.1, 185.2, and 165.9 mAh g^{-1} at the rates of 0.2, 0.5, 1, 2, and even 5 C, respectively, and showed 222.1 mAh g^{-1} even back to 0.2 C. The PMC-only processed electrode had a lower rate capability than the PMC-filtered electrode (containing 3 wt % PVDF) because it contained about 16 wt % PVDF and thus had a lower electrical conductivity. This superior performance indicates that the PVDF layer bonded to the NCM811 particles through the PMC process formed a stable cathode–electrolyte interface to prevent parasitic side reactions and provided high capacity performance and improved cycle stability. Moreover, excess unattached polymers were removed through the filtration process, resulting in stable high capacity performance and high rate capability even at low PVDF content.

To investigate the effect of a thin PVDF layer on the resistance between the NCM811 and the electrolyte, electrochemical impedance spectroscopy (EIS) analysis was performed at 25 °C. The EIS results for the initial, fifth, and 100th cycled states and the resistance values obtained by fitting the impedance spectra are listed in Figures 5 and S8 and Table 1. The Nyquist plots represent the bulk resistance (R_b), the

Table 1. Electrochemical Properties of Simply Mixed and PMC-Filtered NCM/PVDF Electrodes before and after 5 and 100 Cycles Were Obtained from Impedance Spectroscopy

electrodes	cycles	R_b (Ω)	R_{SEI} (Ω)	R_{ct} (Ω)
mix (3 wt %)	0^{th}	8.9		122.8
	5^{th}	9.4	32.2	70.1
	100^{th}	10.5	56.1	83.7
PMC+filter	0^{th}	8.3		52.5
	5^{th}	9.8	33.2	42.5
	100^{th}	10.3	49.6	45.6

solid–electrolyte interface (SEI) film resistance (R_{SEI}), and the charge transfer resistance (R_{ct}) at the interface between the electrode and the electrolyte. Before charging–discharging in Figure 5a, the bulk resistance (R_b) of the PMC-filtered electrode was 8.3 Ω, which was slightly lower than 8.9 Ω of the simply mixed electrode, but similar, because the same amount of binder and the same electrolyte were used. However, the charge transfer resistance (R_{ct}) at the electrode interface of the PMC-filtered electrode was measured to be 52.5 Ω, which is significantly lower than that of the simply mixed electrode of 122.8 Ω. This difference is because the PMC-filtered cathode had a thin and uniform chemically bonded PVDF layer on the NCM particles facilitating Li^+ transport, while the simply mixed cathode had only physically contacted and irregular interfaces between them. After 5 cycles in Figure 5b and 100 cycles in Figure 5c, the R_b of the electrodes prepared by the simple mixing and PMC-filtered process is slightly increased, and a new semicircle appeared due to the SEI layer being newly formed on the lithium metal anode; the obtained R_{SEI} values were 32.2 and 33.2 Ω for 5 cycles and 56.1 and 49.6 Ω for 100 cycles, respectively, indicating similar values. However,

https://doi.org/10.1021/acsaem.2c00244
ACS Appl. Energy Mater. 2022, 5, 4808–4816

the R_{ct} value of the PMC-filtered electrode after 5 and 100 cycles was 42.5 and 45.6 Ω, which slightly increased after the repetitive charge−discharge and was still significantly smaller than the R_{ct} value of the mixed sample of 70.1 and 83.7 Ω. Notably, this smaller R_{ct} value of the PMC-filtered electrode even after 100 cycles indicates that the chemically attached PVDF coating can effectively protect the cathode material from transition metal dissolution and side reactions with the electrolyte and maintain the structural stability of the cathode material. We also acquired the lithium-ion diffusion coefficient (D_{Li^+}) of 100 cycled electrodes by acquiring the Warburg coefficient at low frequency, which can be obtained from the slope of the straight line between the Z' and $\omega^{-1/2}$ axes.[51,52] Figure S9 shows the good linear relationship between Z' and $\omega^{-1/2}$. While D_{Li^+} of the simply mixed electrode was 1.48 × 10^{-11} cm^2 s^{-1}, that of the PMC-filtered electrode was 3.13 × 10^{-11} cm^2 s^{-1}, which is about 2.1 times higher. Therefore, the diffusivity of lithium ions can be effectively enhanced through the PMC process with the PVDF polymers.

It is well-known that NCM particles undergo internal microcracks due to repeated volume changes during long charge−discharge cycles. The propagation of the microcracks reduces the stability of the electrode and increases the interfacial resistance.[53,54] In Figure 5d−f, after cutting the electrode using an ion beam, cross-sectional SEM images were observed to compare the microcrack formation degree of the PMC-filtered and simply mixed (no PMC) electrodes before and after 100 cycles. The internal morphology of the PMC-filtered NCM particles in Figure 5e was well maintained even after 100 cycles without a significant change or microcracks compared to the pristine NCM particles in Figure 5d. However, in the no PMC treated electrode after 100 cycles in Figure 5f, the microcracks considerably propagated to such an extent that cracks separated each domain of the primary particles. In addition, when the element content of the transition metals on the lithium metal electrodes on the opposite side after 100 cycles was analyzed through the EDS mapping (Figures S10 and S11), the transition metal contents were higher in the sample of the simply mixed electrode than in the sample of the PMC filter electrode. On the basis of these results, the PVDF layer with elasticity is conformally and covalently bonded to the NCM particles through the PMC process to prevent microcrack formation even after repeated charging−discharging, which significantly contributes to the excellent cyclability of the cathode.

CONCLUSION

In summary, we introduced the PMC process that simultaneously applies plasma and mechanical friction to the inert PVDF polymers and NCM811 particles to form a uniform polymeric coating layer covalently bonded to the Ni-rich cathode material. In particular, the covalently bonded PVDF layer on the surface of the NCM811 particles serves as an excellent cathode−electrolyte interface that can protect the active material from transition metal dissolution and parasitic side reactions with the electrolyte, which reduces cycling stability and rate capability. In addition, PVDF with high elasticity and high ion conductivity is uniformly coated to the NCM particles, which can significantly improve the structural stability under repetitive volume changes without interfering with lithium-ion transport. Even inert materials without special functional groups can covalently bond to the surface of the cathode material, greatly increasing the degree of freedom of the coating material. Furthermore, since the interfacial stability of the cathode material can be maximized by only the dry composite process, it can be easily applied to the recently issued dry electrode manufacturing process. Lastly, since PVDF used as a binder is attached, an electrode containing only 3 wt % of binder can be fabricated after the filtering process, thereby maximizing energy density without degrading performance. This intimate interaction between NCM particles and PVDF through the PMC process could lead to higher capacity and energy density and better cycling stability and rate capabilities at the cathode of lithium-ion batteries. This PMC process can be a promising approach to overcome the interfacial affinity problem of the recently highlighted dry electrode process and maximize energy storage performance, thereby encouraging innovation in the battery manufacturing process in the future.

ASSOCIATED CONTENT

Supporting Information

The Supporting Information is available free of charge at https://pubs.acs.org/doi/10.1021/acsaem.2c00244.

SEM images of pristine NCM811 and PVDF particles; SEM images with EDS mapping of the PMC-processed composite without plasma treatment before and after the filtration; STEM images of PMC-filtered composites; TGA curve of pristine NCM811 and PMC-processed composites without plasma treatment after filtration; XPS spectra of the PMC+filtered composite, mixed NCM/PVDF composites, and pristine PVDF and NCM811 particles; initial charge−discharge curves of 3% and 20% mixed and PMC-processed and PMC-filtered NCM/PVDF electrodes at 0.5 C; EIS spectra and electrochemical properties (including Warburg coefficient) of simply mixed and PMC-processed electrodes before and after 100 cycles; EDS elemental mapping images of the lithium metal anode with PMC-filtered and simply mixed NCM cathodes (PDF)

AUTHOR INFORMATION

Corresponding Author

Jeong Gon Son − *Soft Hybrid Materials Research Center, Korea Institute of Science and Technology, Seoul 02792, Republic of Korea; KU-KIST Graduate School of Converging Science and Technology, Korea University, Seoul 02841, Republic of Korea;* orcid.org/0000-0003-3473-446X; Email: jgson@kist.re.kr

Authors

Hyein Ko − *Soft Hybrid Materials Research Center, Korea Institute of Science and Technology, Seoul 02792, Republic of Korea; Department of Chemical & Biological Engineering, Korea University, Seoul 02841, Republic of Korea*

Minsung Kim − *Soft Hybrid Materials Research Center, Korea Institute of Science and Technology, Seoul 02792, Republic of Korea; Department of Chemical & Biological Engineering, Korea University, Seoul 02841, Republic of Korea*

Soo Yeong Hong − *Soft Hybrid Materials Research Center, Korea Institute of Science and Technology, Seoul 02792, Republic of Korea*

Jinhan Cho − *Department of Chemical & Biological Engineering and KU-KIST Graduate School of Converging*

Science and Technology, Korea University, Seoul 02841, Republic of Korea; orcid.org/0000-0002-7097-5968

Sang-Soo Lee − *Soft Hybrid Materials Research Center, Korea Institute of Science and Technology, Seoul 02792, Republic of Korea;* orcid.org/0000-0001-5896-6471

Jong Hyuk Park − *Soft Hybrid Materials Research Center, Korea Institute of Science and Technology, Seoul 02792, Republic of Korea;* orcid.org/0000-0002-9554-4523

Complete contact information is available at: https://pubs.acs.org/10.1021/acsaem.2c00244

Notes

The authors declare no competing financial interest.

■ ACKNOWLEDGMENTS

We gratefully acknowledge the financial support from the Korea Institute of Science and Technology (KIST) Institutional Program (Project No. 2E31811), KU-KIST program, and the National Research Foundation of Korea (NRF) grant funded by the Korean government (MEST) (No. 2022R1A2B5B02001597).

■ REFERENCES

(1) Kim, T.; Song, W.; Son, D.-Y.; Ono, L. K.; Qi, Y. Lithium-Ion Batteries: Outlook on Present, Future, and Hybridized Technologies. *J. Mater. Chem. A* **2019**, *7* (7), 2942−2964.

(2) Manthiram, A.; Knight, J. C.; Myung, S.-T.; Oh, S.-M.; Sun, Y.-K. Nickel-Rich and Lithium-Rich Layered Oxide Cathodes: Progress and Perspectives. *Adv. Energy Mater.* **2016**, *6* (1), 1501010.

(3) Kim, J.; Lee, H.; Cha, H.; Yoon, M.; Park, M.; Cho, J. Prospect and Reality of Ni-Rich Cathode for Commercialization. *Adv. Energy Mater.* **2018**, *8* (6), 1702028.

(4) Chakraborty, A.; Kunnikuruvan, S.; Kumar, S.; Markovsky, B.; Aurbach, D.; Dixit, M.; Major, D. T. Layered Cathode Materials for Lithium-Ion Batteries: Review of Computational Studies on $LiNi_{1-x-y}Co_xMn_yO_2$ and $LiNi_{1-x-y}Co_xAl_yO_2$. *Chem. Mater.* **2020**, *32* (3), 915−952.

(5) Myung, S. T.; Maglia, F.; Park, K. J.; Yoon, C. S.; Lamp, P.; Kim, S. J.; Sun, Y. K. Nickel-Rich Layered Cathode Materials for Automotive Lithium-Ion Batteries: Achievements and Perspectives. *ACS Energy Lett.* **2017**, *2* (1), 196−223.

(6) Noh, H. J.; Youn, S.; Yoon, C. S.; Sun, Y. K. Comparison of the Structural and Electrochemical Properties of Layered $Li[Ni_xCo_yMn_z]O_2$ (x = 1/3, 0.5, 0.6, 0.7, 0.8 and 0.85) Cathode Material for Lithium-Ion Batteries. *J. Power Sources* **2013**, *233*, 121−130.

(7) Ryu, H. H.; Park, K. J.; Yoon, C. S.; Sun, Y. K. Capacity Fading of Ni-Rich $Li[Ni_xCo_yMn_{1-x-y}]O_2$ ($0.6 \leq x \leq 0.95$) Cathodes for High-Energy-Density Lithium-Ion Batteries: Bulk or Surface Degradation? *Chem. Mater.* **2018**, *30* (3), 1155−1163.

(8) Zhang, S. S. Problems and Their Origins of Ni-Rich Layered Oxide Cathode Materials. *Energy Storage Mater.* **2020**, *24*, 247−254.

(9) Maleki Kheimeh Sari, H.; Li, X. Controllable Cathode−Electrolyte Interface of $Li[Ni_{0.8}Co_{0.1}Mn_{0.1}]O_2$ for Lithium Ion Batteries: A Review. *Adv. Energy Mater.* **2019**, *9* (39), 1901597.

(10) Ren, X.; Li, Y.; Xi, X.; Liu, S.; Xiong, Y.; Zhang, D.; Wang, S.; Zheng, J. Modification of $LiNi_{0.8}Co_{0.1}Mn_{0.1}O_2$ Cathode Materials from the Perspective of Chemical Stabilization and Kinetic Hindrance. *J. Power Sources* **2021**, *499*, 229756.

(11) Wu, F.; Tian, J.; Su, Y.; Wang, J.; Zhang, C.; Bao, L.; He, T.; Li, J.; Chen, S. Effect of Ni^{2+} Content on Lithium/Nickel Disorder for Ni-Rich Cathode Materials. *ACS Appl. Mater. Interfaces* **2015**, *7* (14), 7702−7708.

(12) Kang, K.; Meng, Y. S.; Bréger, J.; Grey, C. P.; Ceder, G. Electrodes with High Power and High Capacity for Rechargeable Lithium Batteries. *Science (80-.)* **2006**, *311* (5763), 977−980.

(13) Nayak, P. K.; Grinblat, J.; Levi, M.; Levi, E.; Kim, S.; Choi, J. W.; Aurbach, D. Al Doping for Mitigating the Capacity Fading and Voltage Decay of Layered Li and Mn-Rich Cathodes for Li-Ion Batteries. *Adv. Energy Mater.* **2016**, *6* (8), 1502398.

(14) Myung, S. T.; Amine, K.; Sun, Y. K. Surface Modification of Cathode Materials from Nano-to Microscale for Rechargeable Lithium-Ion Batteries. *J. Mater. Chem.* **2010**, *20* (34), 7074−7095.

(15) Chen, Z.; Qin, Y.; Amine, K.; Sun, Y. K. Role of Surface Coating on Cathode Materials for Lithium-Ion Batteries. *J. Mater. Chem.* **2010**, *20* (36), 7606−7612.

(16) Nakhanivej, P.; Park, S. K.; Shin, K. H.; Yun, S.; Park, H. S. Hierarchically Structured Vanadium Pentoxide/Reduced Graphene Oxide Composite Microballs for Lithium Ion Battery Cathodes. *J. Power Sources* **2019**, *436* (March), 226854.

(17) Kwon, M.; Nam, D.; Lee, S.; Kim, Y.; Yeom, B.; Moon, J. H.; Lee, S. W.; Ko, Y.; Cho, J. Textile-Type Lithium-Ion Battery Cathode Enabling High Specific/Areal Capacities and High Rate Capability through Ligand Replacement Reaction-Mediated Assembly. *Adv. Energy Mater.* **2021**, *11* (36), 2101631.

(18) Dong, M.; Wang, Z.; Li, H.; Guo, H.; Li, X.; Shih, K.; Wang, J. Metallurgy Inspired Formation of Homogeneous Al_2O_3 Coating Layer To Improve the Electrochemical Properties of $LiNi_{0.8}Co_{0.1}Mn_{0.1}O_2$ Cathode Material. *ACS Sustain. Chem. Eng.* **2017**, *5* (11), 10199−10205.

(19) Han, B.; Key, B.; Lapidus, S. H.; Garcia, J. C.; Iddir, H.; Vaughey, J. T.; Dogan, F. From Coating to Dopant: How the Transition Metal Composition Affects Alumina Coatings on Ni-Rich Cathodes. *ACS Appl. Mater. Interfaces* **2017**, *9* (47), 41291−41302.

(20) Han, B.; Paulauskas, T.; Key, B.; Peebles, C.; Park, J. S.; Klie, R. F.; Vaughey, J. T.; Dogan, F. Understanding the Role of Temperature and Cathode Composition on Interface and Bulk: Optimizing Aluminum Oxide Coatings for Li-Ion Cathodes. *ACS Appl. Mater. Interfaces* **2017**, *9* (17), 14769−14778.

(21) Schipper, F.; Bouzaglo, H.; Dixit, M.; Erickson, E. M.; Weigel, T.; Talianker, M.; Grinblat, J.; Burstein, L.; Schmidt, M.; Lampert, J.; Erk, C.; Markovsky, B.; Major, D. T.; Aurbach, D. From Surface ZrO_2 Coating to Bulk Zr Doping by High Temperature Annealing of Nickel-Rich Lithiated Oxides and Their Enhanced Electrochemical Performance in Lithium Ion Batteries. *Adv. Energy Mater.* **2018**, *8* (4), 1701682.

(22) Li, L.; Xu, M.; Yao, Q.; Chen, Z.; Song, L.; Zhang, Z.; Gao, C.; Wang, P.; Yu, Z.; Lai, Y. Alleviating Surface Degradation of Nickel-Rich Layered Oxide Cathode Material by Encapsulating with Nanoscale Li-Ions/Electrons Superionic Conductors Hybrid Membrane for Advanced Li-Ion Batteries. *ACS Appl. Mater. Interfaces* **2016**, *8* (45), 30879−30889.

(23) Xie, J.; Sendek, A. D.; Cubuk, E. D.; Zhang, X.; Lu, Z.; Gong, Y.; Wu, T.; Shi, F.; Liu, W.; Reed, E. J.; Cui, Y. Atomic Layer Deposition of Stable $LiAlF_4$ Lithium Ion Conductive Interfacial Layer for Stable Cathode Cycling. *ACS Nano* **2017**, *11* (7), 7019−7027.

(24) Song, H. G.; Kim, J. Y.; Kim, K. T.; Park, Y. J. Enhanced Electrochemical Properties of $Li(Ni_{0.4}Co_{0.3}Mn_{0.3})O_2$ Cathode by Surface Modification Using Li_3PO_4-Based Materials. *J. Power Sources* **2011**, *196* (16), 6847−6855.

(25) Zhao, E.; Chen, M.; Hu, Z.; Xiao, X.; Chen, D. Layered/Layered Homostyructure Ion Conductor Coating Strategy for High Performance Lithium Ion Batteries. *Electrochim. Acta* **2016**, *208*, 64−70.

(26) Ju, S. H.; Kang, I.; Lee, Y.; Shin, W.-K.; Kim, S.; Shin, K.; Kim, D. Improvement of the Cycling Performance of $LiNi_{0.6}Co_{0.2}Mn_{0.2}O_2$ Cathode Active Materials by a Dual-Conductive Polymer Coating. *ACS Appl. Mater. Interfaces* **2014**, *6* (4), 2546−2552.

(27) Xiong, X.; Ding, D.; Wang, Z.; Huang, B.; Guo, H.; Li, X. Surface Modification of $LiNi_{0.8}Co_{0.1}Mn_{0.1}O_2$ with Conducting Polypyrrole. *J. Solid State Electrochem.* **2014**, *18* (9), 2619−2624.

(28) Chen, S.; He, T.; Su, Y.; Lu, Y.; Bao, L.; Chen, L.; Zhang, Q.; Wang, J.; Chen, R.; Wu, F. Ni-Rich $LiNi_{0.8}Co_{0.1}Mn_{0.1}O_2$ Oxide Coated by Dual-Conductive Layers as High Performance Cathode

Material for Lithium-Ion Batteries. *ACS Appl. Mater. Interfaces* **2017**, *9* (35), 29732−29743.
(29) Song, L.; Tang, F.; Xiao, Z.; Cao, Z.; Zhu, H.; Li, A. Enhanced Electrochemical Properties of Polyaniline-Coated $LiNi_{0.8}Co_{0.1}Mn_{0.1}O_2$ Cathode Material for Lithium-Ion Batteries. *J. Electron. Mater.* **2018**, *47* (10), 5896−5904.
(30) Wang, D.; Wang, X.; Yang, X.; Yu, R.; Ge, L.; Shu, H. Polyaniline Modification and Performance Enhancement of Lithium-Rich Cathode Material Based on Layered-Spinel Hybrid Structure. *J. Power Sources* **2015**, *293*, 89−94.
(31) Chang, B.; Kim, J.; Cho, Y.; Hwang, I.; Jung, M. S.; Char, K.; Lee, K. T.; Kim, K. J.; Choi, J. W. Highly Elastic Binder for Improved Cyclability of Nickel-Rich Layered Cathode Materials in Lithium-Ion Batteries. *Adv. Energy Mater.* **2020**, *10* (29), 2001069.
(32) Cao, Y.; Qi, X.; Hu, K.; Wang, Y.; Gan, Z.; Li, Y.; Hu, G.; Peng, Z.; Du, K. Conductive Polymers Encapsulation To Enhance Electrochemical Performance of Ni-Rich Cathode Materials for Li-Ion Batteries. *ACS Appl. Mater. Interfaces* **2018**, *10* (21), 18270−18280.
(33) Beyer, M. K.; Clausen-Schaumann, H. Mechanochemistry: The Mechanical Activation of Covalent Bonds. *Chem. Rev.* **2005**, *105* (8), 2921−2948.
(34) James, S. L.; Adams, C. J.; Bolm, C.; Braga, D.; Collier, P.; Friščic, T.; Grepioni, F.; Harris, K. D. M.; Hyett, G.; Jones, W.; Krebs, A.; Mack, J.; Maini, L.; Orpen, A. G.; Parkin, I. P.; Shearouse, W. C.; Steed, J. W.; Waddell, D. C. Playing with Organic Radicals as Building Blocks for Functional Molecular Materials. *Chem. Soc. Rev.* **2012**, *41* (1), 413−447.
(35) Do, J. L.; Friščić, T. Mechanochemistry: A Force of Synthesis. *ACS Cent. Sci.* **2017**, *3* (1), 13−19.
(36) Amrute, A. P.; De Bellis, J.; Felderhoff, M.; Schüth, F. Mechanochemical Synthesis of Catalytic Materials. *Chem. - A Eur. J.* **2021**, *27* (23), 6819−6847.
(37) You, J.; Kim, J. H.; Seo, K. H.; Huh, W.; Park, J. H.; Lee, S. S. Implication of Controlled Embedment of Graphite Nanoplatelets Assisted by Mechanochemical Treatment for Electro-Conductive Polyketone Composite. *J. Ind. Eng. Chem.* **2018**, *66*, 356−361.
(38) You, J.; Lee, Y. M.; Choi, H. H.; Kim, T. A.; Lee, S. S.; Park, J. H. Thermally Stable and Highly Recyclable Carbon Fiber-Reinforced Polyketone Composites Based on Mechanochemical Bond Formation. *Compos. Part A: Appl. Sci. Manuf.* **2021**, *142*, 106251.
(39) You, J.; Choi, H. H.; Cho, J.; Son, J. G.; Park, M.; Lee, S. S.; Park, J. H. Highly Thermally Conductive and Mechanically Robust Polyamide/Graphite Nanoplatelet Composites via Mechanochemical Bonding Techniques with Plasma Treatment. *Compos. Sci. Technol.* **2018**, *160*, 245−254.
(40) You, J.; Choi, H. H.; Lee, Y. M.; Cho, J.; Park, M.; Lee, S. S.; Park, J. H. Plasma-Assisted Mechanochemistry to Produce Polyamide/Boron Nitride Nanocomposites with High Thermal Conductivities and Mechanical Properties. *Compos. Part B: Eng.* **2019**, *164*, 710−719.
(41) Lin, C.; Yang, L.; Ouyang, L.; Liu, J.; Wang, H.; Zhu, M. A New Method for Few-Layer Graphene Preparation via Plasma-Assisted Ball Milling. *J. Alloys Compd.* **2017**, *728*, 578−584.
(42) Dong, Z.; Peng, Y.; Zhang, X.; Xiong, D. B. Plasma Assisted Milling Treatment for Improving Mechanical and Electrical Properties of In-Situ Grown Graphene/Copper Composites. *Compos. Commun.* **2021**, *24*, 100619.
(43) Dou, S.; Tao, L.; Wang, R.; El Hankari, S.; Chen, R.; Wang, S. Plasma-Assisted Synthesis and Surface Modification of Electrode Materials for Renewable Energy. *Adv. Mater.* **2018**, *30* (21), 1705850.
(44) Wang, Y.; Yang, L.; Hu, R.; Sun, W.; Liu, J.; Ouyang, L.; Yuan, B.; Wang, H.; Zhu, M. A Stable and High-Capacity Anode for Lithium-Ion Battery: Fe_2O_3 Wrapped by Few Layered Graphene. *J. Power Sources* **2015**, *288*, 314−319.
(45) Yang, H. M.; Kwon, Y. K.; Lee, S. B.; Kim, S.; Hong, K.; Lee, K. H. Physically Cross-Linked Homopolymer Ion Gels for High Performance Electrolyte-Gated Transistors. *ACS Appl. Mater. Interfaces* **2017**, *9* (10), 8813−8818.
(46) Wang, Y.; Huang, K.; Zhang, P.; Li, H.; Mi, H. PVDF-HFP Based Polymer Electrolytes with High Li^+ Transference Number Enhancing the Cycling Performance and Rate Capability of Lithium Metal Batteries. *Appl. Surf. Sci.* **2022**, *574*, 151593.
(47) Chen, G.; Zhang, F.; Zhou, Z.; Li, J.; Tang, Y. A Flexible Dual-Ion Battery Based on PVDF-HFP-Modified Gel Polymer Electrolyte with Excellent Cycling Performance and Superior Rate Capability. *Adv. Energy Mater.* **2018**, *8* (25), 1801219.
(48) Vandencasteele, N.; Reniers, F. Plasma-Modified Polymer Surfaces: Characterization Using XPS. *J. Electron Spectrosc. Relat. Phenom.* **2010**, *178−179* (C), 394−408.
(49) Bayer, B. C.; Bosworth, D. A.; Michaelis, F. B.; Blume, R.; Habler, G.; Abart, R.; Weatherup, R. S.; Kidambi, P. R.; Baumberg, J. J.; Knop-Gericke, A.; Schloegl, R.; Baehtz, C.; Barber, Z. H.; Meyer, J. C.; Hofmann, S. In Situ Observations of Phase Transitions in Metastable Nickel (Carbide)/Carbon Nanocomposites. *J. Phys. Chem. C* **2016**, *120* (39), 22571−22584.
(50) Cho, E.; Kim, M.; Park, J.; Lee, S.-J. Plasma-Polymer-Fluorocarbon Thin Film Coated Nanostructured-Polyethylene Terephthalate Surface with Highly Durable Superhydrophobic and Antireflective Properties. *Polymers* **2020**, *12* (5), 1026.
(51) Zhang, X.; Ma, F.; Wei, G.; Lei, Z.; Qu, J. Improvement of Electrochemical Performance of $LiNi_{0.8}Co_{0.1}Mn_{0.1}O_2$ Cathode Material via $Li_{2.09}W_{0.9}Nb_{0.1}O_4$ Li-Ion Conductive Coating Layer. *J. Solid State Electrochem.* **2020**, *24* (10), 2301−2313.
(52) Choi, W.; Shin, H.-C.; Kim, J. M.; Choi, J.-Y.; Yoon, W.-S. Modeling and Applications of Electrochemical Impedance Spectroscopy (EIS) for Lithium-Ion Batteries. *J. Electrochem. Sci. Technol.* **2020**, *11* (1), 1−13.
(53) Bak, S.; Hu, E.; Zhou, Y.; Yu, X.; Senanayake, S. D.; Cho, S.; Kim, K.; Chung, K. Y.; Yang, X.; Nam, K. Structural Changes and Thermal Stability of Charged $LiNi_xMn_yCo_z$ O_2 Cathode Materials Studied by Combined In Situ Time-Resolved XRD and Mass Spectroscopy. *ACS Appl. Mater. Interfaces* **2014**, *6* (24), 22594−22601.
(54) Yang, J.; Xia, Y. Suppressing the Phase Transition of the Layered Ni-Rich Oxide Cathode during High-Voltage Cycling by Introducing Low-Content Li_2MnO_3. *ACS Appl. Mater. Interfaces* **2016**, *8* (2), 1297−1308.

https://doi.org/10.1021/acsaem.2c00244
ACS Appl. Energy Mater. 2022, 5, 4808−4816